Efficient Composite Colorization of Copper by Spatially Controlled Oxidation with Deep-UV Ultrafast Lasers

Baptiste Groussin, Miguel Martinez-Calderon, Oihane Beldarrain, Ainara Rodriguez, Santiago M. Olaizola, Bruce A. Marsh, and Eduardo Granados*

Colorizing metals using micrometer and nanometer scale surface modifications has been vastly investigated and presents many advantages for applications across scientific and technological fields. By tuning the surface chemical composition or controlling its morphology, it is possible to produce a wide range of chromatic effects. Ultrafast laser processing presents here an interesting asset, as it allows to simultaneously provide chemical and morphological modifications at the micro-scale in a single step. In this article, the composite colorization of copper surfaces with mW-class average power deep ultraviolet (DUV) femtosecond laser pulses is demonstrated. The advantages of this setup are twofold: first, thanks to the increased absorption of copper in the DUV, the technique allows scaling down the requirement for laser power. Second, under ultrafast short-wavelength illumination molecular oxygen bond-breaks occur, enhancing the oxidation rate of the copper. The technique allows for highly controllable and efficient copper oxidation with the irradiation parameters. Taking these two effects into account, the generation of a wide spectrum of colors—from dark blue to shiny red—is demonstrated, and the role of the surface oxidation rate, the laser fluence, and laser scanning strategies in the colorization of copper surfaces employing DUV lasers is discussed.

1. Introduction

In recent years, methods for coloring metals without the need for complex industrial chemical processing have become attractive as they can provide an environmentally friendly, low-cost alternative to traditional chemical paints. Standard ink-based methods cannot easily produce durable colors because of the difficulty of adhering paints to polished metallic surfaces, while high spatial resolution and energy-efficient solutions are challenges still to be overcome. An ink-less coloring method represents a key alternative that does not require material transport, supply chains, or industrial processes, and hence reduces the overall impact on the environment. Coloring copper is particularly interesting due to its well-known characteristics, such as high electrical and thermal conductivity, making it ubiquitous in its microelectronic and power electronics industries.[1] Copper can also be laser printed into flexible wearable materials,[2] however, a non-invasive, non-destructive, and ultra-precise technique for coloring its delicate surface remains elusive.

Technologies for color variation exploiting nanofeatures and interference effects have been actively studied for applications in sensors,[3,4] displays,[5,6] and manufacturing industries, including the printing of serial numbers, barcodes, company logos, and anti-counterfeiting measures.[7] Surface coloring using lasers, with a remarkable throughput exceeding mm^2 s^{-1}, presents an enticing solution to surmount this challenge.[8–10] Moreover, lasers have the capability to perform large-scale fabrication on surfaces with significant roughness, a task that proves challenging for traditional methods like electron beam lithography and nanoimprinting.[11]

Two types of ink-less coloring can be distinguished: First, surface-structural coloring is based on the production of micro- or nanometric morphological features that interact with light in various ways. For example, it is possible to tailor the absorption spectrum and hence the perceived colors of a copper surface by employing plasmonic effects in optimized 3D nano-geometries.[12–19] Alternatively, periodic structures that mimic diffraction gratings can also produce iridescent colors if the condition given by Bragg's law is met for visible light.[20–24] Second, altering the chemical composition of a surface without using chemical substances can be achieved using lasers,[25–27] as a way to effectively fabricate a highly adhesive thin-film that will give rise to colors via interferometric effects, hence modifying

B. Groussin, M. Martinez-Calderon, B. A. Marsh, E. Granados
CERN
European Organization for Nuclear Research
Geneva 1211, Switzerland
E-mail: eduardo.granados@cern.ch
O. Beldarrain, A. Rodriguez, S. M. Olaizola
CEIT - Basque Research and Technology Alliance (BRTA)
Manuel Lardizabal 15, Donostia, San Sebastián 20018, Spain
O. Beldarrain, A. Rodriguez, S. M. Olaizola
Tecnun, Universidad de Navarra
Manuel Lardizabal 13, Donostia, San Sebastián 20018, Spain

ADVANCED
SCIENCE NEWS

www.advancedsciencenews.com

ADVANCED
OPTICAL
MATERIALS

www.advopticalmat.de

the reflectance spectrum of the metal. Oxide layers constitute one of the most suitable options for the production of thin-films on copper, for it is well-known that this metal easily oxidizes and produces robust, long-lasting oxide layers.[28–32]

The chemical mechanism of copper oxidation is well understood,[33] and several methods allow fabricating such films with high accuracy and reproducibility.[34,35] Although an ideal thin-film deposition method like atomic sputtering or epitaxial growth may produce results of unrivaled homogeneity,[28] extensive environment control and vacuum requirements render this approach complex. In this respect, laser-based copper oxide thin-film fabrication methods provide an easy, in-air alternative with high precision down to the diffraction limit.[36–39] Laser processing of surfaces can be performed easily on flexible and 3D objects and requires no additional components whatsoever.[40,41] However, the work conducted so far with infrared laser photo-oxidation sometimes presents several undesirable side-effects, like the fabrication of laser induced periodic surface structures (LIPSS) that inevitably produce a strong angle-dependency of the coloring of the surface via diffraction.[31,42]

In this paper, we address these limitations by performing efficient photo-oxidation with a femtosecond laser in the DUV range at 257 nm. The increase in photon energy improves the oxidation rate by approaching the bond dissociation energy of molecular oxygen,[43] while the increased absorption cross-section of copper allows for effective localized heat deposition. The combination of these two effects yields enhanced oxidation rates using laser pulses with nJ energy at mW average powers. Ultrashort laser pulses enable high peak powers to be reached, as required for efficient molecular dissociation, thereby making the oxide production via non-thermal effects overall more efficient. In addition, the lowered diffraction limit in the DUV also allows for smaller spot sizes for processing with high accuracy on the sub-micron scale. Conveniently, the nanostructures produced by localized surface Plasmon polaritons (LSPP) such as LIPSS have a spatial periodicity that does not allow diffraction of visible light, hence inhibiting the production of iridescent coloring. We have developed a nanomachining setup, allowing us to investigate a wide range of fabrication parameters, including scanning speed, pitch distance, and laser energy. We obtain a wide range of vibrant colors covering nearly the entire visible spectrum, from the shiny golden-orange look of polished copper to the typical light green tone of cuprous oxide (Cu_2O), passing by deep-blue and purple colors. The coloring here is achieved due to interferometric effects in the oxide layer and is tuned with its thickness. We study the processed surfaces using optical profilometry and characterize the elemental content of the surface via energy dispersive X-ray spectroscopy (EDX).

2. Theory

The fast oxidation process of a metallic surface during laser irradiation can be broken down to five distinct steps:[20,29] 1) heating of the metal due to the relaxation of electron energy excited by the laser; 2) at high temperature the reaction between oxygen and the metal is enabled by the physical adsorption of oxygen on the copper surface; 3) dissociation of the oxygen bonds in the air around the surface by laser photons and ionic liaison formation between copper ions and oxygen free electrons;

4) lateral growth of the oxide germ producing a thin metal oxide film; and 5) perpendicular growth of the metallic oxide layer by cation/anion charge diffusion. Copper oxide primarily exists in either of the two known stoichiometric forms: Cu_2O and CuO, corresponding to cubic and monoclinic crystal structures and known as cuprous and cupric oxide, respectively. The copper oxidation mechanism and the composition of surface oxide layers formed at different temperatures have been extensively studied in the literature[44] and it was shown that an oxide layer formed under low or ambient oxygen pressure and temperatures below 300 °C contains predominantly Cu_2O. Analogously, it has been shown that the oxidation produced by laser beams is mainly dominated by the cuprous type,[45] although mixtures of both oxides usually coexist.[33] This is relevant for our coloring application because cupric oxides present large optical absorption at visible wavelengths, which is beneficial for some applications such as coatings for solar panels,[46] but for our application it will decrease the overall color brightness.
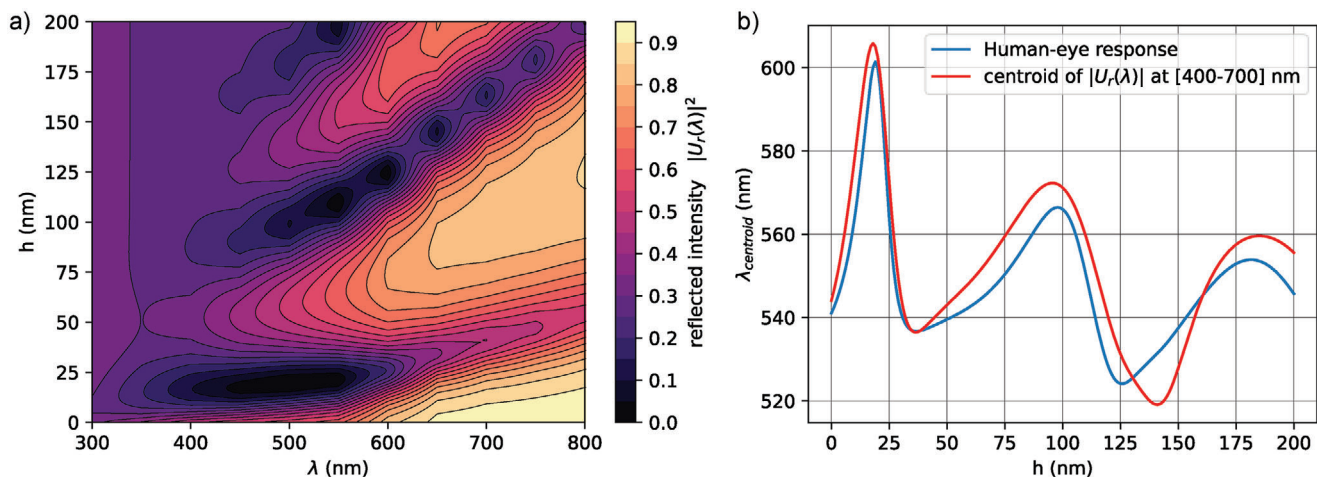
In terms of the resulting overall chromatic and optical response, two main aspects shall be taken into account, namely: the layer thickness and its composition, and its spatial distribution. For our calculations, we assume a configuration consisting of a semiconductor cuprous oxide layer of variable thickness over a copper polished substrate since it retrieves optimal coloring results. The simulation was carried out by modeling the system as a Fabry-Perot cavity with complex reflection and transmission coefficients calculated using Fresnel equations, a technique similar to calculating the structural color response of Gires–Tournois cavities[38] and ultra thin-films[26,47] but with a lossy copper back-reflector in our case. In this arrangement, the total reflected wave amplitude can be calculated as[48]

$$U_r(\lambda) = r_1 + \frac{t_1 t'_1 r'_2 e^{i\phi}}{1 - r'_1 r'_2 e^{i\phi}} \quad (1)$$

where r_1 and t_1 are the complex amplitude reflectance and transmittance of the air-oxide interface, analogously r'_1 and t'_1 are for the oxide-air interface, and r'_2 is the complex reflectance of the oxide-pure copper interface. At normal incidence, the resulting expressions for reflectance and transmittance are simply $r_1 = (1 - n_{Cu_2O})/(1 + n_{Cu_2O})$, $t_1 = 2/(1 + n_{Cu_2O})$, $r'_1 = (n_{Cu_2O}-1)/(1 + n_{Cu_2O})$, $t'_1 = 2n_{Cu_2O}/(1 + n_{Cu_2O})$, and $r'_2 = (n_{Cu_2O}-n_{Cu})/(n_{Cu_2O}+n_{Cu})$. We use here the complex refractive index $n(\lambda)$ to account for the spectral absorption in both the copper and oxide layers. ϕ is the phase accumulated between successive reflections due to the oxide layer of thickness h and the angle of incidence θ, and can be calculated using the expression

$$\phi = 4\pi\nu \frac{n_0(\lambda)h}{c} \cos(\theta) \quad (2)$$

ν corresponds to the frequency of the impinging light, and $n_0(\lambda)$ is the real part of the complex index of refraction of the oxide layer. For the values of the index of refraction n_0 and extinction coefficient κ of copper and cuprous oxide in the visible spectral range, we used the ones reported in refs. [49] and [50], respectively. The specific model results for the experimental arrangements are included in **Figure 1**a, where we show the calculations of the spectral reflectivity $|U_r(\lambda)|^2$ of ideal Cu_2O layers. Figure 1b

**ADVANCED
SCIENCE NEWS**

www.advancedsciencenews.com

**ADVANCED
OPTICAL
MATERIALS**

www.advopticalmat.de

Figure 1. a) Computed spectral reflectivity in the visible range of a copper surface covered by a thin layer of Cu_2O of thickness h. b) Centroid of the reflected spectrum calculated for the visible spectral range (400–700 nm) and for the human eye spectral response.

shows the centroid of the reflected spectrum calculated in the range 400–700 nm as well as taking into account the human eye response (modeled as a Gaussian sensitivity profile centered at 555 nm with a FWHM of 150 nm corresponding to photopic vision under well-lit conditions).

The calculations were performed using Equation (1) and with the purpose of qualitatively supporting the experimental observations. The specific values for complex index of refraction of copper and copper oxides are included in Supporting Information. An analogous calculation can be performed for other forms of copper oxide (such as CuO), although they do not produce a modulated visible color reflectance as in the cuprous oxide case, as it is mostly absorptive. In reality, the resulting oxide layer will contain both oxide types, and so it is possible to calculate the overall results by estimating the effective refractive index and extinction coefficient using a mixing rule, such as the effective medium approximation (EMA) or Maxwell–Garnett equation. These mixing rules take into account the refractive indices, extinction coefficients, and volume fractions of the individual oxides to calculate the effective properties of the mixture. The simulations show that for cuprous oxide layers of about 10–25 nm, 80–125 nm, and around 190 nm, the reflectivity in the green–yellow spectral range is heavily suppressed. We suggest that this is the mechanism by which the appearance of the sample gains blue and purple tones. For layers of thickness between 40–50 and 125–175 nm the reflectivity at green wavelengths is clearly increased, producing the typical green copper oxide color.

In terms of the spatial distribution of the oxide layer, the laser-based deposition technique is generally in-homogeneous at micron scales due to the typical Gaussian profile of the laser beam as well as the dynamic ablated depth while processing. However, since the laser spot used is only a few microns, the composite result of different layer thickness across the surface in a relatively small area produces a homogeneous color effect as perceived by the human naked eye, which can only recognize objects down to around 50 µm. This allows us to carefully adjust the rastering pitch s (spacing between adjacent grooves), speed v, and laser fluence F_0 simultaneously to produce a homogeneous-looking broad palette of colors, even

though the deposition of the oxide layer is in-homogeneous at the micron scale.

3. Experimental Section

The schematic of the setup is depicted in **Figure 2a**. Here the use of ultrashort pulses of DUV 257 nm photons of energy E = 4.8 eV brought numerous advantages to this scheme. First, the photon energy was placed above the work function of Cu (4.7 eV). This, combined with the high energy density of ultrashort laser pulses, ensured an increased absorption cross-section of the copper surface. Second, the sub-picosecond timescales of ultrafast beams also enabled fast electron heating without much lattice diffusion, implying optimal electron excitation without cumulative heating and surface melting, which favored the production of colorful cuprous oxides. Finally, singlet oxygen (O_2) in air atmosphere presented double-bonds having a dissociation energy above 5 eV.[43] Thus, a two-photon excitation will break bonds efficiently and provide a higher influx of oxygen ions to the oxidation reaction. Overall, more oxygen ions and an increased affinity of the metallic surface result in the quicker growth of a thin-film copper oxide layer. Therefore, DUV photo-oxidation presented interesting potential gains for producing efficient oxide layers on copper.

A high repetition rate Yb:KGW laser source from Light Conversion was used for the copper surface processing setup, which is depicted in Figure 2b. The laser was capable of delivering up to 6 W average power at 1030 nm, with a pulse duration between 190 fs and 10 ps at up to 200 kHz repetition rate. In order to produce a DUV beam, second and fourth harmonic conversion stages were used based on beta barium borate (BBO) crystals to reach a final wavelength of 257 nm. The DUV energy was precisely adjusted in a range between 300 and 10 nJ by rotating a motorized $\lambda/2$ waveplate to tune the amount of S-polarized light transmitted through a thin film polarizer (TFP). The average power deposited on the sample did not exceed 10 mW in any of the experiments performed. The S-polarized beam is then steered toward a UV femtosecond-grade 100 mm focal length lens and focused on the copper sample surface with a spot size ω
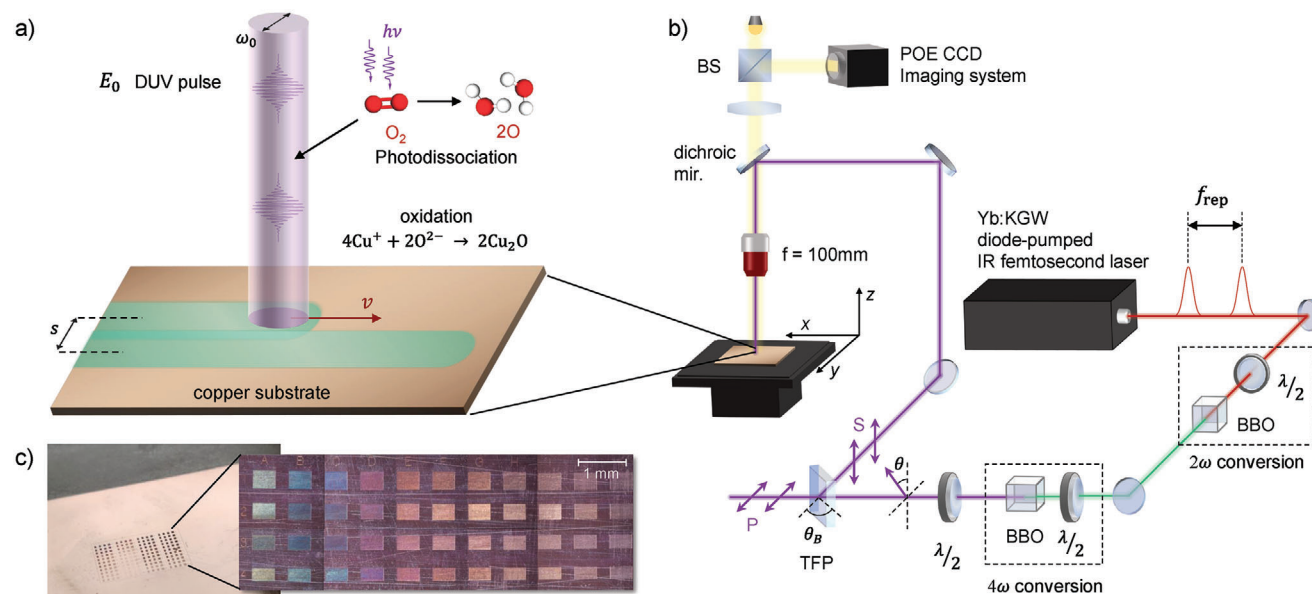
Figure 2. a) Photo-oxidation process schematic showing DUV ultrashort pulses irradiating the surface, with insets showing the dissociation of oxygen molecules and copper oxidation reaction. b) Experimental optical setup featuring an IR femtosecond laser, its harmonic conversion to DUV, the nanopositioning stage for sample handling, and the imaging system. c) Image of the nanostructured sample as seen by the naked eye (left) and with a low magnification microscope (right), showing the produced colors as they appear under ambient light.

of 10 μm ($1/e^2$). Patterning the surface with sub-micron accuracy was achieved by moving the sample using a three-axis motorized stage with down to 200 nm repeatability. Finally, a microscope imaging system placed on top of the machining line was used to have live visual feedback over the machining operations at the few-micron scale.

The samples used for this study were $80 \times 80 \times 5$ mm^3 square foils of oxygen-free high thermal conductivity (OFHC) copper that were polished via diamond turning down to Ra 10 nm. Prior to laser treatment, the samples were rinsed in an ultrasonic bath with a 15 g L^{-1} alkaline solution at 50 °C for 20 min. The next step was an immersion-cleaning in de-mineralized water, followed by a spray cleaning with ethyl alcohol to aid in the drying process. Finally, the foils were dried with pressurized nitrogen and stored in a low-vacuum desiccator before and after the laser treatment.

The machining analysis was performed rastering the ultrafast laser over the copper: arrays of lines were scanned at constant speed but with variable inter-spacing or pitch s between the lines over areas of 500×300 μm^2 as shown in Figure 2a,c. The repetition rate of the laser was set to $f_{rep} = 10$ kHz, the IR output pulse energy of 90 μJ and spot size ω of 10 μm were fixed at these values during the study. A series of rectangles featuring different combinations of fluence F_0 and number of overlapping pulses N, by changing the DUV pulse energy E_0 and the translation stage speed v, were produced. These two variables were grouped by sorting the results in terms of cumulative energy deposited per unit area, namely the dose D in J cm^{-2}, taking into account the mean single-pulse laser fluence F_0 multiplied by the effective number of overlapping pulses N, and defined as

$$D = F_0 \times N = \frac{E_0}{\pi \omega_0^2} \times \frac{f_{rep} 2\omega}{v} \tag{3}$$

where ω is the beam spot size, f_{rep} and v account for the overlap of consecutive pulses along a line during machining, increasing the total laser energy impinging the surface.

4. Results

The laser processed areas were characterized by analyzing their surface morphology, color (both at the micro- and macro-scales), and elemental composition. To this end, an optical profilometer (S neox from Sensofar Metrology) was used to obtain the reflected chromatic information from the processed areas. This device uses a confocal microscope capable of capturing high resolution images of surfaces by illuminating the sample with calibrated sources of white, red, blue, and green light at normal incidence.

Examples of colored surfaces are shown in **Table 1**, where it can be easily observed that the resulting color is dependent mostly on the integrated dose D for a fixed pitch distance s of 12 μm. It should be noted, however, that D is not the only parameter defining the resulting color. The combination of dose D, processing speed v and pitch distance s ultimately defines the result.

Figure 3a shows arrays of machined areas using low-magnification, summarizing the results obtained in terms of different laser machining parameters. The coloring effect occurred for a pulse peak fluence F_0 between 10 and 20 mJ cm^{-2} for all tested values of N. Three single pulse energies E_0 were tested: 61, 43, and 34 nJ which cover the range between the ablation threshold of copper and the low fluence regime.[51] We then explored scanning speeds v from 50 μm s^{-1} to 3 mm s^{-1} and pitch distance s for a range of deposited doses D between 2.58 and 54.74 J cm^{-2}. The pitch was set to $s = 6$, 8, 10, and 12 μm. We observed that within this finely-tuned range of D, the laser processing of copper generates bright and homogeneous colors, going from a shiny

2302071 (4 of 8)

Table 1. Color images showing the evolution of machined copper surfaces with the increasing dose D, as a function of the single pulse fluence F_0 and the number of pulses N for a constant pitch s of 12 µm.

F_0 (mJ cm^{-2})	19.41	19.41	10.82	19.41	13.68	19.41	10.82	13.68	10.82	13.68	10.82	13.68
N	133	266	100	666	1000	1000	2000	2000	2666	2666	4000	4000
D (J cm^{-2})	2.58	5.17	10.82	12.94	13.68	19.41	21.64	27.37	28.86	36.49	43.29	54.74
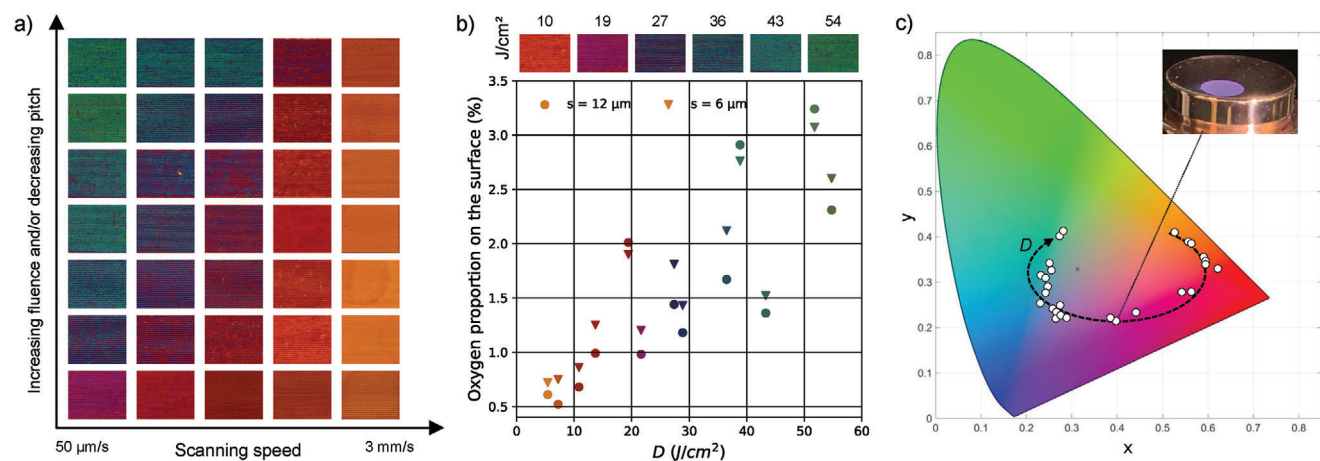
Figure 3. a) Obtained colors as a function of processing scanning speed, pitch s, and fluence F_0. b) Measured oxygen content of the laser-processed areas as a function of integrated dose D for pitch distances of $s = 6$ and 12 µm. c) Commission Internationale de L'Eclairage (CIE) xy chromaticity diagram with our averaged colors over the processed areas with different laser processing parameters. The arrow indicates the trajectory of the produced color as a function of integrated dose D. (inset) Laser-processed copper surface showcasing vivid purple colors for values of D in the range of 19–36 J cm^{-2}.
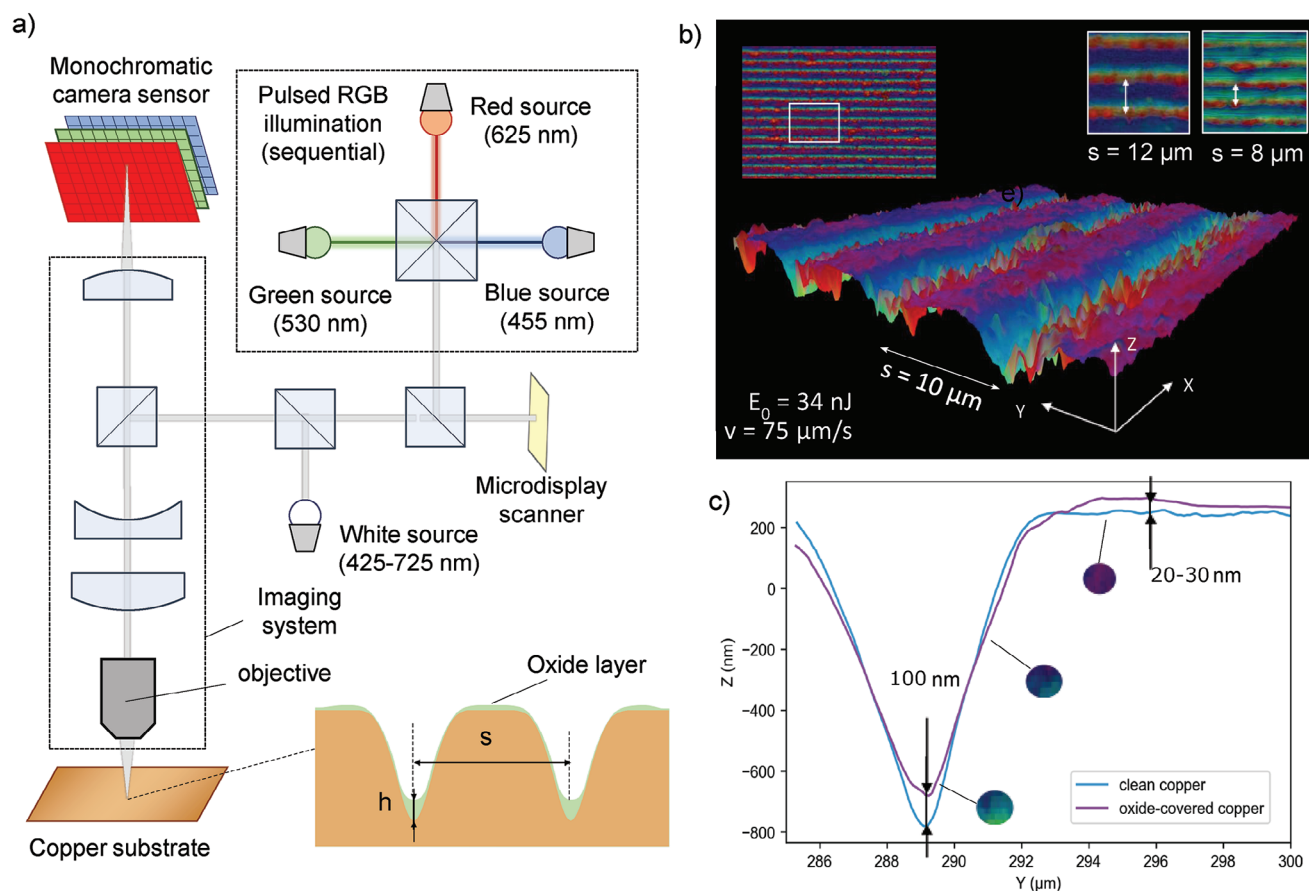
yellow/gold to a light green tone and passing by deep blue and purple. To the naked eye, the perceived colors were independent of the viewing angle. Further information regarding the expected angle dependency as well as pictures at different angles of the produced colors can be found in Section S3.2, Supporting Information.

The results of this 3D scan are projected onto two dimensions in Figure 3a to highlight the composite effect of our coloring approach: while the colors at the local µm level present strong differences, the overall perceived color depends on a combination of pitch and fluence and scanning speed. To some extent, the results show that these variables are exchangeable; for example, a blue-purple tone is achievable using either a slow scanning speed at low fluence and large pitch or at high speed, high fluence, and small pitch. Ultimately, the choice of optimum parameters for producing a desired color depends on the characteristics of the laser and positioning stages utilized, and here we only portray the interchangeability of the machining parameters. The pitch s does not seem to have a significant effect on the coloring at the µm scale, that is, colors inside the grooves measured at large microscope magnifications essentially stay constant for different pitches, but it is crucial for the resulting composite color. The scanning speed v has the most impact on the evolution of color at the micron scale, as it changes rapidly the total number of incident pulses and hence the integrated dose D.

For the oxide content analysis, a scanning electron microscope (SEM) equipped with an EDX allowed us to study the surface

morphology and estimate the chemical composition at the elemental level at sub-micron scales. Figure 3b shows the results of the oxygen content (integrated across the penetration depth of the electron beam into the sample) for different values of D. For integrated doses D above 50 J cm^{-2} the oxygen content dominates the resulting color of the sample (typical green color from cuprous oxides). The linear trend of the oxygen content as a function of integrated dose D showcases the controllability of our coloring technique. The oxygen content inside each laser-produced groove was independent of the pitch s, meaning that there was no substantial formation of oxide from the adjacent laser passes. Moreover, as the number of pulses N was increased further, the oxidized area became clearly green, supporting the hypothesis that cuprous oxide formation dominates at low temperatures, while at higher temperatures, cupric oxide is dominant. Additional results are included in Supporting Information. It is worth noting the appearance of nanostructures for a narrow window of integrated dose, mostly occurring at lower fluence than the reported values of Cu surface nano-patterning with longer wavelength fs-lasers[52] and even UV wavelengths.[53]

The resulting surface-averaged colors were mapped in the Commission Internationale de L'Eclairage XYZ space of coordinates, plotted in Figure 3c. Here, we computed the mean spectrum over the entire surface of the processed areas of a few mm^2. The colors evolve from yellow to green gradually with an increased D, ranging from 10–54 J cm^{-2}. For very low doses, the resulting color is red–orange as expected for untreated cop-

**ADVANCED
SCIENCE NEWS**

www.advancedsciencenews.com

**ADVANCED
OPTICAL
MATERIALS**

www.advopticalmat.de

Figure 4. a) Schematic of the measurement device (Sensofar S Neox) featuring sequential pulsed illumination at 455, 530, and 625 nm. (inset) Schematic cross-section of a laser-processed area, indicating the oxide layer thickness h and pitch s. b) Example of a topographic map overlaid with the local surface color of a sample processed with 34 nJ pulses at a speed of 75 µm s^{-1} and a pitch of 10 µm. (inset) Two examples of processed surfaces with the same laser parameters but different pitch s of 8 and 12 µm, highlighting the composite effect of the perceived color as a function of groove interspacing. c) Results of the profilometer depth measurement for the same processing parameters before and after removing the oxide layer, indicating its thickness at various locations.

per surfaces. As the dose is increased, the reflected spectra become purple, followed by blue and then turquoise. For the highest dose, the color produced is mostly green. Notably, colors produced using our technique cover about half of the area of the standard red/green/blue (sRGB) color space, which is similar to the capabilities reported using other more complex oxidation mechanisms,[28] and still much larger coverage than that obtained using plasmonic effects.[12]

To further analyze the process, we conducted a study of the color composition of these matrices and the oxide layer thickness using optical microscope profilometry before and after removing the oxide layer. **Figure 4** shows the concept behind composite coloring using variable spatially distributed oxide layer thicknesses: while the deposited oxide layer can be thicker at the groove deepest point, its thickness varies around the groove and toward its sides resulting in a perceived averaged color. To this end, the optical profilometer allowed us to simultaneously obtain the reflected chromatic information from the processed areas at micron scales while simultaneously measuring the depth with nanometer resolution. This device uses a confocal microscope capable of capturing high-resolution topographic and true-color images of sur-

faces by illuminating them sequentially with calibrated sources of white, red (625 nm), blue (455 nm), and green (530 nm) light at normal incidence, as shown in Figure 4a.

Figure 4b shows the 3D topography overlaid with the reflected color measured at each sample location. The result shows how the reflected color varies gradually as a function of lateral distance y from the deepest point inside each groove at micrometric scales, from green to turquoise, then blue and purple. This color gradient arises from a variable oxide thickness deposition during the laser processing. In the inset of Figure 4b we show resulting "true color" microscope images, for equivalent laser processing parameters but with pitches s of 8 and 12 µm. We performed depth measurements of the samples before and after removing the oxide layers, taking reference points outside the grooves for the off-set height compensation.

The oxide layers were removed using a mask and a monoethyleneglycol (MEG) solvent, the residual chemicals on the copper surface were negligible after the clean-up. An example of a profilometer trace before and after the oxide removal is shown in Figure 4c, where a thickness between 20 and up to 100 nm was observed. This range of thickness results in colors ranging from

**ADVANCED
SCIENCE NEWS**

www.advancedsciencenews.com

**ADVANCED
OPTICAL
MATERIALS**

www.advopticalmat.de

violet at the highest point to greenish at the deepest point, with variable thickness at the edges. The results agree reasonably well with the expected from simulations: for a layer of around 100 nm there is a decrease in the reflectivity at wavelengths above 500 nm, resulting in a turquoise color. A layer of thickness 20–30 nm produces analogously an increased reflectivity in the spectral range below 400 nm, yielding a purple–blue color. It is worth noting that the same coloring effect can be obtained with thicker layers, as the spectral response of the thin-film is periodic to some extent, but with lower brightness due to increased absorption. While the accuracy of the profilometer was about 0.1 nm in depth, the method used for adjusting the overall height of the sample had an accuracy of around 10 nm, and therefore the depths indicated in Figure 4c are only approximated to that level. The depth profiles for the tested parameters can be found in the supporting information. The results show that our technique is highly reproducible over large areas, as seen in the regularity of the color distribution across the grooves. Further analyses were realized 1 year after laser processing of the samples, and no deterioration of the coloring of the copper surfaces was observed. An additional EDX analysis (included in the Supporting Information) was conducted to quantify the amount of oxygen content variation over one year, resulting in a negligible increase in its concentration. This indicates that the produced colors can be considered stable in years time-scales.

5. Discussion and Conclusion

We have demonstrated a composite coloring scheme for copper attributed to progressive and spatially tailored oxidation using DUV lasers. Fast and intense heating of the surface and excitation of the dioxygen molecules in the vicinity of the surface are responsible for breaking chemical bonds and combining ions into CuO and Cu_2O groups at the surface. Generally, it can be stated that the more laser doses is sent to the surface, the higher the oxidation rate. We studied surface composition at the nano-scale by EDX to measure the oxide proportion in the surface composition, the results show a concentration going from 0.5% to 3.5% of oxide. The evolution of color can be explained by a progressive accumulation of oxide at the surface, aiming toward green which is the typical color of copper-oxide surfaces. Shiny yellow, on one side of the spectrum, is obtained through very low fluence laser processing. Then a progressive increase in D shows a clear rise in oxide rate and an evolution of the observed color toward blue and then green. The micron-precision spatially distributed oxide layer, in which the thickness is modulated by the integrated dose, opens the doorway to highly controllable composite coloring of copper surfaces.

Deep UV laser surface processing of copper is interesting as it enables the coloring of its surface with enhanced control. The coloring process is shown to require significantly lower fluence than other wavelength ranges (enabling speedy large area processing) and offers a high degree of flexibility and reliability as it does not produce angle-dependent coloring results. Fast developments of laser technologies promises that such methods for surface coloring might become increasingly popular in the upcoming years thanks to their efficiency and precision. Our technique offers significant advantages over standard ink-based methods including the very good spatial resolution due to the spot size

scale while avoiding the use of consumable materials like chemical ink or paints in the coloring process. In this sense, the main technological edge of a purely oxide-based coloring approach is the expected color stability over time as oxide layers are usually chemically stable, although further investigations would have to be done in that matter.

In conclusion, achieving a large gradient of vivid colors is straightforward with the current DUV ultrafast laser technologies by simply tuning machining parameters such as scanning speed or focused spot size, by adapting the integrated dose with micro-meter resolution. We believe the technique will be highly relevant for coloring applications in materials exhibiting non-flat, delicate and flexible surfaces, where precision and durability are key aspects.

Supporting Information

Supporting Information is available from the Wiley Online Library or from the author.

Conflict of Interest

The authors declare no conflict of interest.

Data Availability Statement

The data that support the findings of this study are available from the corresponding author upon reasonable request.

Keywords

coloring, copper, photo-oxidation, ultrafast

[1] M. Singh, S. Rana, *Mater. Today Commun.* **2020**, *24*, 101317.

[2] Z. Li, S. Chang, S. Khuje, S. Ren, *ACS Nano* **2021**, *15*, 6211.

[3] X. Zhang, C. Liu, L. Zhang, L. Jia, M. Shi, L. Chen, Y. Di, Z. Gan, *Adv. Funct. Mater.* **2021**, *31*, 2010406.

[4] M. Xiong, Y. Sheng, Y. Di, F. Xing, L. Yu, J. Zhang, W. Zhou, C. Liu, L. Dong, Z. Gan, *ACS Appl. Mater. Interfaces* **2021**, *13*, 33566.

[5] X. Duan, S. Kamin, N. Liu, *Nat. Commun.* **2017**, *8*, 14606.

[6] D. Franklin, R. Frank, S.-T. Wu, D. Chanda, *Nat. Commun.* **2017**, *8*, 15209.

[7] J. Xue, Z.-K. Zhou, Z. Wei, R. Su, J. Lai, J. Li, C. Li, T. Zhang, X.-H. Wang, *Nat. Commun.* **2015**, *6*, 8906.

[8] X. Zhu, C. Vannahme, E. Højlund-Nielsen, N. A. Mortensen, A. Kristensen, *Nat. Nanotechnol.* **2016**, *11*, 325.

[9] X. Cui, X. Zhu, L. Shao, J. Wang, A. Kristensen, *Adv. Opt. Mater.* **2020**, *8*, 1901605.

[10] Y. Wang, F. Ren, T. Ding, *Adv. Opt. Mater.* **2020**, *8*, 2000164.

[11] J. Geng, L. Xu, W. Yan, L. Shi, M. Qiu, *Nat. Commun.* **2023**, *14*, 565.

[12] J.-M. Guay, A. Calà Lesina, G. Côté, M. Charron, D. Poitras, L. Ramunno, P. Berini, A. Weck, *Nat. Commun.* **2017**, *8*, 16095.

[13] J. C. Blake, S. Rossi, M. P. Jonsson, A. Dahlin, *Adv. Opt. Mater.* **2022**, *10*, 2200471.

[14] P. Fan, M. Zhong, L. Li, P. Schmitz, C. Lin, J. Long, H. Zhang, *J. Appl. Phys.* **2014**, *115*, 124302.

[15] P. Fan, M. Zhong, L. Li, P. Schmitz, C. Lin, J. Long, H. Zhang, *J. Appl. Phys.* **2013**, *114*, 083518.

[16] E. M. Garcell, C. Guo, *Opt. Mater. Express* **2019**, *9*, 1033.

[17] X. Wang, A. Kuchmizhak, D. Storozhenko, S. Makarov, S. Juodkazis, *ACS Appl. Mater. Interfaces* **2018**, *10*, 1422.

[18] R. Feng, H. Wang, Y. Cao, Y. Zhang, R. J. H. Ng, Y. S. Tan, F. Sun, C.-W. Qiu, J. K. W. Yang, W. Ding, *Adv. Funct. Mater.* **2022**, *32*, 2108437.

[19] Y. Lin, Z. Chen, L. Fang, M. Meng, Z. Liu, Y. Di, W. Cai, S. Huang, Z. Gan, *Nanotechnology* **2018**, *30*, 015402.

[20] E. Amara, F. Haïd, A. Noukaz, *Appl. Surf. Sci.* **2015**, *351*, 1.

[21] Y. Liu, S. Li, S. Niu, X. Cao, Z. Han, L. Ren, *Appl. Surf. Sci.* **2016**, *379*, 230.

[22] J. Long, P. Fan, M. Zhong, H. Zhang, Y. Xie, C. Lin, *Appl. Surf. Sci.* **2014**, *311*, 461.

[23] Z. Ou, M. Huang, F. Zhao, *Opt. Express* **2014**, *22*, 17254.

[24] M. Iqbal, V. Ialyshev, V. Kim, G. Boltaev, D. Ivanov, B. Rethfeld, R. A. Ganeev, A. S. Alnaser, *Appl. Sci.* **2020**, *10*, 6207.

[25] S. Wang, T. Ding, *J. Mater. Chem. C* **2019**, *7*, 13410.

[26] T. Ding, *J. Mater. Chem. C* **2020**, *8*, 10825.

[27] S. Wang, J. Yao, X. Lu, T. Ding, *Adv. Opt. Mater.* **2022**, *10*, 2102238.

[28] S. J. Kim, S. Kim, J. Lee, Y. Jo, Y.-S. Seo, M. Lee, Y. Lee, C. R. Cho, J.-p. Kim, M. Cheon, J. Hwang, Y. I. Kim, Y.-H. Kim, Y.-M. Kim, A. Soon, M. Choi, W. S. Choi, S.-Y. Jeong, Y. H. Lee, *Adv. Mater.* **2021**, *33*, 2007345.

[29] H. Liu, W. Lin, M. Hong, *APL Photonics* **2019**, *4*, 051101.

[30] J. Geng, L. Xu, W. Yan, L. Shi, M. Qiu, *Nat. Commun.* **2023**, *14*, 565.

[31] G. Killaire, J. Walia, S. Rashid, P. Berini, A. Weck, *Appl. Surf. Sci.* **2022**, *583*, 152440.

[32] E. M. Garcell, S. C. Singh, H. Li, B. Wang, S. A. Jalil, C. Guo, *Nanoscale Adv.* **2020**, *2*, 2958.

[33] C. Gattinoni, A. Michaelides, *Surf. Sci. Rep.* **2015**, *70*, 424.

[34] M. A. M. Patwary, M. A. Hossain, B. C. Ghos, J. Chakrabarty, S. R. Haque, S. A. Rupa, J. Uddin, T. Tanaka, *RSC Adv.* **2022**, *12*, 32853.

[35] M. Galbiati, A. C. Stoot, D. M. A. Mackenzie, P. Bøggild, L. Camilli, *Sci. Rep.* **2017**, *7*, 39770.

[36] M. Wautelet, *Appl. Phys. A* **1990**, *50*, 131.

[37] H. Palneedi, J. H. Park, D. Maurya, M. Peddigari, G.-T. Hwang, V. Annapureddy, J.-W. Kim, J.-J. Choi, B.-D. Hahn, S. Priya, K. J. Lee, J. Ryu, *Adv. Mater.* **2018**, *30*, 1705148.

[38] T. Guo, Z. Liu, Y. Jin, N. Wang, Z. Zhang, S. He, *Adv. Opt. Mater.* **2022**, *10*, 2101546.

[39] H. Zhao, Q. Zhang, Y. Hou, Z. Cheng, T. Xia, S. Cao, P. Wang, *Opt. Laser Technol.* **2023**, *159*, 109040.

[40] F. Huang, Z. Yan, S. Zhou, B. Gu, S. Wang, S. Wang, S. Zhou, *Opt. Express* **2023**, *31*, 8190.

[41] M.-L. Huang, Z. Cai, Y.-Z. Wu, S.-G. Lu, B.-S. Luo, Y.-H. Li, *Vacuum* **2020**, *178*, 109489.

[42] T. T. D. Huynh, A. Petit, N. Semmar, *Appl. Surf. Sci.* **2014**, *302*, 109.

[43] Z. Farooq, D. A. Chestakov, B. Yan, G. C. Groenenboom, W. J. van der Zande, D. H. Parker, *Phys. Chem. Chem. Phys.* **2014**, *16*, 3305.

[44] L. B. Boinovich, K. A. Emelyanenko, A. G. Domantovsky, E. V. Chulkova, A. A. Shiryaev, A. M. Emelyanenko, *Adv. Mater. Interfaces* **2018**, *5*, 1801099.

[45] L. Baufay, F. A. Houle, R. J. Wilson, *J. Appl. Phys.* **1987**, *61*, 4640.

[46] A. Bhaumik, A. Haque, P. Karnati, M. Taufique, R. Patel, K. Ghosh, *Thin Solid Films* **2014**, *572*, 126.

[47] M. A. Kats, F. Capasso, *Laser Photonics Rev.* **2016**, *10*, 735.

[48] W. H. Steel, *Interferometry*, 2nd ed., Cambridge University Press, Cambridge **1986**.

[49] W. S. M. Werner, K. Glantschnig, C. Ambrosch-Draxl, *J. Phys. Chem. Ref. Data* **2009**, *38*, 1013.

[50] C. G. Ribbing, A. Roos, in *Handbook of Optical Constants of Solids* (Ed.: E. D. Palik), Academic Press, Burlington **1997**, pp. 875–882. https://www.sciencedirect.com/science/article/pii/B9780125444156500856.

[51] S. Nolte, C. Momma, H. Jacobs, A. Tünnermann, B. N. Chichkov, B. Wellegehausen, H. Welling, *J. Opt. Soc. Am. B* **1997**, *14*, 2716.

[52] Y. Fuentes-Edfuf, J. A. Sánchez-Gil, C. Florian, V. Giannini, J. Solis, J. Siegel, *ACS Omega* **2019**, *4*, 6939.

[53] T. Bukelis, E. Gaižauskas, O. Balachninaitė, D. Paipulas, *Surf. Interfaces* **2023**, *38*, 102869.